Title
Deletion of a remote enhancer near ATOH7 disrupts retinal neurogenesis, causing NCRNA disease

Authors
Ghiasvand, Noor M
Rudolph, Dellaney D
Mashayekhi, Mohammad
et al.

Peer reviewed

Deletion of a remote enhancer near *ATOH7* disrupts retinal neurogenesis, causing NCRNA disease

Noor M. Ghiasvand[1,2], **Dellaney D. Rudolph**[3], **Mohammad Mashayekhi**[4], **Joseph A. Brzezinski IV**[3,6], **Daniel Goldman**[5], and **Tom Glaser**[3,*]

[1] Neuroscience Research Center and Department of Medical Genetics, School of Medicine, Shahid Beheshti University of Medical Sciences, Tehran, Iran

[2] Department of Biology, Grand Valley State University, Allendale, MI 49401

[3] Department of Human Genetics and Internal Medicine, University of Michigan, Ann Arbor, MI 48109

[4] Ophthalmology Ward, Emam Ali Hospital, Bojnourd, North Khorasan, Iran

[5] Molecular and Behavioral Neuroscience Institute, Department of Biochemistry, University of Michigan, Ann Arbor, MI 48109

Abstract

Individuals with nonsyndromic congenital retinal nonattachment (NCRNA) are totally blind from birth. The disease afflicts ~1% of Kurdish people living in a group of neighboring villages in North Khorasan, Iran. We show NCRNA is caused by a 6523bp deletion that spans a remote *cis* regulatory element 20 kb upstream from *ATOH7* (*Math5*), a bHLH transcription factor gene required for retinal ganglion cell (RGC) and optic nerve development. In humans, the absence of RGCs stimulates massive neovascular growth of fetal blood vessels within the vitreous, and early retinal detachment. The remote *ATOH7* element appears to act as a secondary or 'shadow' transcriptional enhancer. It has minimal sequence similarity to the primary enhancer, which is close to the *Atoh7* promoter, but drives transgene expression with an identical spatiotemporal pattern in the mouse retina. The human transgene also functions in zebrafish, reflecting deep evolutionary conservation. These dual enhancers may reinforce *Atoh7* expression during early critical stages of eye development when retinal neurogenesis is initiated.

Keywords

nonsyndromic congenital retinal nonattachment (NCRNA); persistent hyperplastic primary vitreous (PHPV); retinal ganglion cell (RGC); optic nerve hypoplasia; retinopathy of prematurity

*Author for correspondence: Tom Glaser, University of Michigan Medical Center, 2047 BSRB, Box 2200, 109 Zina Pitcher Place, Ann Arbor, MI 48109-2200, tel 734-764-4580, fax 734-763-2162, tglaser@umich.edu.
[6]Current address: Department of Biological Structure, University of Washington, Seattle, WA 98195

(ROP); *Math5*; retinal cell fate specification; corneal blood staining; conserved noncoding element (CNE); shadow enhancer; Iranian Kurds; basic helix-loop-helix (bHLH); retinal dysgenesis; blindness; *ATOH7*; neurogenesis; hyaloid vasculature; falciform fold; genomic evolution; RNANC

INTRODUCTION

The vertebrate neural retina develops during embryogenesis from multipotent progenitors in the optic cup. These cells exit mitosis and differentiate to form photoreceptors, interneurons, Müller glia, and retinal ganglion cells (RGCs) through the actions of intrinsic and extrinsic factors[1]. Seven major cell types emerge from the progenitor pool in a relatively fixed order, with overlapping birthdates, and differentiate to form a highly laminar structure that detects and processes visual information. Histogenesis starts in the central retina and spreads to the periphery over several days to weeks, depending on the species. Ganglion cells are the first-born retinal neurons in all vertebrates and occupy the innermost nuclear layer. Their axons comprise the optic nerves, which convey all visual information from the eyes to the brain. In mice, RGC genesis begins on embryonic day E11 and peaks around E13. In humans, RGCs are born between the 5th and 11th weeks of gestation. In addition to neurons, the retina contains astrocytes, which originate from a separate progenitor pool in the optic stalk. These enter the eye during late gestation, migrate across the inner retinal surface, and retain mitotic potential[2].

Intrinsic factors controlling retinal histogenesis have been defined in large part through analysis of mouse genetic models. An archetypal example is the proneural bHLH (basic helix-loop-helix) transcription factor Atoh7 (Math5), a homolog of *Drosophila* Atonal[3]. The *Atoh7* gene is transiently expressed in newly post-mitotic precursors, beginning with the onset of neurogenesis[4]. *Atoh7* mutant mice lack optic nerves and have a >95% reduction in ganglion cell abundance[5],[6]. No other cell type is missing. Their eyes detect light and process visual information within the retina but transmit few, if any, signals to the brain[7]. An orthologous *ath5* mutation was identified in the *lakritz* zebrafish[8]. In mouse *Cre-lox* lineage experiments, *Atoh7*+ precursors give rise to 5% of cells in the normal adult retina, but only a fraction of these precursors develop as RGCs[4],[9]. *Atoh7* thus acts as a competence factor for RGC fate. Differentially expressed mRNAs have been identified in mutant retinas[10], but the exact mechanism of Atoh7 action is incompletely understood.

The mammalian retina is nourished by two vascular systems. The inner two-thirds is supplied by the central artery, which enters the eye through the optic nerve and branches to form surface and deep capillary beds. The outer retina is oxygenated by diffusion from the surrounding choriocapillaris. Both systems derive from the fetal circulation[11],[12]. In the embryo, inner hyaloid and outer ciliary vessels envelop the optic cup, anastomose across the rim, and fill the vitreous space. Starting at P0 in mice, vessels surrounding the lens regress through a branch-wise process of apoptosis, and the hyaloid trunk is remodeled to form the central retinal artery. In humans, these events occur during late gestation and early postnatal life[13].

Many forms of hereditary blindness are caused by mutations in genes required for retinal cell maintenance or physiology, leading to slow or rapidly progressing degeneration[14]. A smaller number of diseases involve genes such as *CRX* or *NR2E3*, which are required for photoreceptor differentiation[15]. As yet, no human retinal disorder has been specifically associated with defects in fate determination of non-photoreceptor cell types. Congenital retinal vascular disorders are also major causes of blindness worldwide. In retinopathy of prematurity (ROP), familial exudative vitreoretinopathy (FEVR) and persistent hyperplasia of the primary vitreous (PHPV), ischemia and angiogenic signaling defects are the primary stimulus for pathological retinal neovascularization[11].

Congenital retinal nonattachment is a severe form of blindness, with no detection of light from birth[16]. The retina is partially or completely separated from the posterior globe, and there is typically a fibrovascular mass behind the lens. The disease is heterogeneous, with a variety of clinical and histological anomalies involving the retina and blood vessels in one or both eyes. In some patients, the disease occurs with systemic malformations, but there is no consistent association. Sporadic and familial cases have been reported[17]. A nonsyndromic hereditary form (NCRNA) is common in North Khorasan, Iran, among descendants of a Kurdish founder population, and it is inherited as an autosomal recessive trait with complete penetrance[18]. The locus was mapped by SSLP linkage and haplotype analysis to a 0.6–1.5 cM region on chromosome 10q21, but the causative mutation and pathogenic mechanism are unknown[19],[20]. In principle, the disease could arise from an intrinsic flaw in neuronal or vascular development.

In this report, we show that blind NCRNA patients lack optic nerves, which prevents light perception and profoundly affects the development of retinal vasculature. Our data suggest that NCRNA is caused by deletion of conserved DNA sequences that appear to control *ATOH7* expression in early neuroretinal precursors. Finally, we show that the deleted sequences have properties consistent with a duplicate or 'shadow' enhancer[21], including: [1] an identical pattern of transcriptional activation as the primary *Atoh7* enhancer, [2] a remote genomic location, [3] a comparatively recent evolutionary origin and [4] conserved biological activity among vertebrates. NCRNA is thus a Mendelian is order that disrupts the intrinsic mechanism of retinal cell fate determination.

RESULTS

Nonsyndromic congenital retinal nonattachment (NCRNA)

This autosomal recessive disorder (MIM221900) was first described in a large consanguineous Kurdish family that traces its ancestry for nine generations (Fig. 1g). The founders were dislocated centuries ago from Kurdistan to North Khorasan province in eastern Iran, during the Safavid Dynasty[22], and their descendants remained relatively isolated, linguistically, culturally and genetically, from the main Persian population until recent years. The disease afflicts 1.1% of the population in four neighboring villages, with an estimated carrier frequency of 18% for the NCRNA allele[18].

The affected individuals are totally blind, with no perception of light. Their eyes exhibit leukocoria (white pupils), esotropia (misalignment with inward deviation), and a continuous

pendular nystagmus (jerky eye movements) (Fig. 1a–f). The pupils have no direct or consensual light reaction. In three-quarters of eyes examined, the anterior chambers were relatively shallow, but there was no consistent elevation of intraocular pressure. During a previous study[18], B-scan ultrasonography and serial fundoscopic examinations revealed formation of a dense mass behind the lens in each eye, with complete opacification of the vitreous by four months (Fig. 1e,f). There is also a slowly progressive corneal clouding, consistent with endothelial blood staining[23], which was evident to some extent in all adults examined. This develops over several years, is more severe in the inferior part of the cornea (Fig. 1b), and may occur with iridocorneal adhesions. No other sensory or neurological defects have been detected in the blind individuals. Their auditory, olfactory, endocrine and intellectual functions are intact, and they have normal developmental milestones. They have no systemic or other vascular abnormalities. Together, these clinical findings suggest bilateral persistence of the fetal blood vessels, with complete congenital detachment of the neural retina, and intravitreal vascular proliferation during infancy. The obligate heterozygotes are clinically normal. They have good vision, with no structural or functional eye pathology.

Optic nerve aplasia in NCRNA

Given the complete blindness, congenital nystagmus, and absent pupillary light reflexes, we investigated optic nerve defects as the primary anatomical basis for NCRNA pathology. Nystagmus is common in children with severe optic nerve malformations[24], and it is thought to arise from unbalanced sensory input to central autonomic centers controlling gaze, and a failure to calibrate oculomotor systems. The pupillary light reflex is triggered by rare photosensitive RGCs, which relay signals to the cortex of the olivary pretectal nuclei via the optic nerves. Proximity of the NCRNA region to *ATOH7* also raised the possibility of optic nerve involvement. *Atoh7* mutant mice have essentially no pupillary reflex[25], and significant retinovascular abnormalities[26], although retinal detachments are rare.

In the original fundoscopic exams of one affected infant prior to vitreal opacification, the status of the optic discs could not be determined[18]. To characterize the optic nerves anatomically, we performed orbital MRI exams on one adult NCRNA patient (Fig. 2a–c,f). As expected, this study showed heterogeneous consolidation of the vitreous compartments, consistent with complete retinal detachment and a retrolental fibrovascular mass in each eye. The sclerae (white fibrous outer layer of the eye globes), lens, extraocular muscles, retrobulbar fat and adnexa (lacrimal glands and other accessory visual structures) appeared relatively normal, and there were no anatomical defects in the anterior brain. In contrast, the optic nerves and chiasm were absent or greatly attenuated in multiple views. However, because the oculomotor and ciliary nerves and ophthalmic blood vessels were difficult to resolve within the orbital cones, we cannot exclude the presence of small atrophic optic nerves in these patients, similar to residual RGCs reported in some *Atoh7* mutant mice[27].

Identification of the NCRNA mutation

The critical region spans 1639kb, from *D10S1670* to *D10S1418*, and overlaps 14 positional candidate genes, including *ATOH7* (Fig. 3a). We therefore tested blind (rr) and heterozygous (Rr) family members for mutations in the *ATOH7* transcription unit[28],[29] and known

regulatory elements within 5.5kb of the initiation site, by sequencing multiple PCR amplicons (Supplementary Fig. 1, Supplementary Table 1). The proximal 1.8kb upstream segment has been conserved during vertebrate evolution[28] and is sufficient to drive reporter transgene expression in embryonic mouse retinas with a pattern similar to the *Math5-lacZ* knock-in allele[30],[31].

No sequence changes were found in the *ATOH7* gene or proximal upstream region compared to the NCBI reference genome or known variants. Likewise, no mutation was found in any of the 13 other genes in the nonrecombinant interval, including *SIRT1*, which has a major retinal dysgenesis phenotype in mutant mice (Supplementary Table 2).

To screen for remote structural changes in the *ATOH7* region, we amplified single-copy DNA products from the 74 kb intergenic segment delimited by flanking genes *PBLD* (phenazine biosynthesis-like domain) and *MYPN* (myopalladin). This analysis revealed a deletion of six adjacent amplicons out of 17 distributed across the region, in samples from blind individuals (rr) compared to non-carrier relatives (RR) (Fig. 3, Supplementary Table 3). To verify this result and define endpoints, we performed multiple PCRs with primers flanking the deletion, and amplified a nested set of junctional products from NCRNA samples (Supplementary Fig. 2). The deletion spans 6523bp, with 5bp microhomology at the endpoints (Fig. 4b). It is located 21.7 to 15.2kb upstream of the *ATOH7* transcription start site and 28.8 to 35.3kb downstream from the 3′ end of *PBLD* (Fig. 3c). We then genotyped all available samples from the pedigree (n =150), including individuals who were not part of the original linkage studies, using a triplex strategy to amplify wild-type (+) and NCRNA ( ) alleles simultaneously (Fig. 4a). The results were completely concordant with phenotype data. All 31 blind individuals were homozygous for the deletion (   ), and all 119 sighted relatives were homozygous for the wild-type allele (++, n = 39) or heterozygous for the deletion (+, n = 80, including known obligate carriers). The correlation is highly significant ($\chi^2 = 150.17$ for $df = 3$, giving $P = 1.20 \times 10^{-32}$).

To evaluate the small possibility of a second, coincidental deletion or duplication in the nonrecombinant region, we performed high-resolution SNP (single nucleotide polymorphism) analysis on six DNA samples from the NCRNA pedigree, including two blind patients and two obligate carriers (Supplementary Fig. 3). This analysis detected the deletion 20kb upstream from *ATOH7* (spanning rs385145) but no further abnormalities. Unexpectedly, DNA from one blind individual (10877) was heterozygous for SNP markers centromeric to *MYPN*, revealing a novel recombinant disease haplotype. The underlying crossover narrows the critical region to 713kb and formally excludes four of the original candidate genes. Although an occult point mutation is theoretically possible, the combined genetic, clinical and functional data strongly support a causal relationship between the 6.5 kb deletion and NCRNA disease.

The NCRNA deletion removes a cis regulatory element

Since heterozygotes are healthy, a loss of gene function is the most logical pathogenic mechanism. The deleted region contains no annotated exons, cDNAs or ESTs (Fig. 3c). In principle, the 6.5 kb deletion could affect expression of *ATOH7*, *PBLD* or a more distant

gene. Dysregulation of *PBLD* is an unlikely explanation for NCRNA disease pathology, because it is not expressed in the developing eye (see below).

To rigorously survey the expression of flanking genes, we performed RT-PCR analysis in mice (Supplementary Fig. 4). Although a low level of *Mypn* mRNA was detected in the fetal eye, only *Atoh7* is specifically expressed at high levels. Because EST and 5′RACE data provide no evidence for an alternative upstream exon or mRNA splicing[29], these results are most consistent with an enhancer mutation affecting the transcriptional regulation of *ATOH7*.

The NCRNA deletion removes a cluster of three conserved noncoding elements (CNEs) with a level of nucleotide identity among mammals that is comparable to the *ATOH7* coding and proximal regulatory regions (Fig. 3c). To test the function of these CNEs *in vivo*, we generated transgenic mice in which 3.8 kb human genomic DNA from the deletion was joined to a minimal β-globin promoter (BG) and red fluorescent protein (nuclear Cherry) reporter (Fig. 5). This 3034-BGnCherry transgene was specifically expressed in the developing retina in 5 of 6 founder embryos and 2 of 3 stable lines. No activity was detected from the remaining two integration events. The restricted spatiotemporal pattern matches the *Math5-lacZ* knock-in allele, beginning at E11.5 with the onset of retinal neurogenesis and continuing to P1 in newly post-mitotic retinal precursors[4],[5] (Fig. 6a,b,e–). No overlap was observed between nuCherry and the S-phase marker BrdU or the M-phase marker PH3 (Fig. 6c,d,f–h). Together, our data suggest the deleted CNEs may act as a transcriptional enhancer. These CNEs are further upstream from the *ATOH7* coding sequence than previously studied regions[32]. Although not tested directly, the NCRNA deletion may impair the level or timing of *ATOH7* expression.

Functional comparison of genomic enhancers near *ATOH7*

The mammalian *ATOH7* region contains two broad regulatory units–a primary enhancer located within 2kb of the promoter, which has been characterized in mouse genomic DNA[30],[31], and the remote cluster of CNEs that is deleted in the NCRNA pedigree (Fig. 5). To directly compare their activities, we crossed 3034-BGnCherry and Math5-GFP mice, which carry reporters controlled by the human remote and mouse primary enhancers respectively, and examined nuCherry and GFP expression in double transgenic embryos by fluorescence and confocal microscopy, and flow cytometry (Fig. 7, Supplementary Fig. 5). These patterns were essentially overlapping, spatially and temporally, despite the fact that regulatory elements in the transgenes were derived from different species, that the primary and remote regulatory units have little sequence similarity to each other (Supplementary Figs. 6–8), and that *Atoh7* is only transcribed for a few hours in each cell, beginning after terminal M phase. Flow analysis of dissociated E14.5 neural retinas revealed a single population of cells, comprising 40% of the total, that coexpress nuCherry and GFP (and presumably *Atoh7*) (Fig. 7c). There were few single-positive cells, which could arise from differences in folding time and perdurance of the reporter proteins. Thus, despite devastating clinical consequences of the NCRNA deletion (Figs. 1–2), the proximal and remote enhancers appear redundant in their ability to direct transcription in a transgenic context.

Unlike the coding region, which is deeply conserved among vertebrates, there is limited sequence homology between the remote enhancer, in mouse or human DNA, and the corresponding region upstream of *Atoh7* (*ath5*) in teleosts (Supplementary Figs.7–8). Indeed, the syntenic block containing *Atoh7* has been significantly disrupted by evolutionary chromosome rearrangements with breakpoints close to the promoter (Supplementary Fig. 6). To test enhancer function in a divergent species, we generated *3034-BGnCherry* zebrafish carrying the same nuCherry reporter transgene. In these fish, nuCherry expression was restricted to the developing retina and correlated with the onset of neurogenesis (Fig. 8a,b). Moreover, *3034-BGnCherry* fully overlapped expression of the *ath5:GFP* transgene[33] which contains 7kb zebrafish *Atoh7* regulatory DNA (Fig. 8c,d and Supplementary Fig. 9). Although distantly related by structure and ancestry, the human remote enhancer is appropriately recognized by transcriptional machinery in the teleost retina and is thus functionally conserved.

DISCUSSION

In this paper, we identify an *ATOH7* regulatory deletion as the probable cause of nonsyndromic congenital retinal nonattachment, a Mendelian disorder of cell fate determination. Although circumstantial, this conclusion is based on the most parsimonious interpretation of concordant phenotypic, genetic, transgene expression and evolutionary data. Since *Atoh7* controls development of the first-born retinal neurons (RGCs), the deleted enhancer, and the proximal regulatory region, appear to be the principal sites in the mammalian genome responsible for initiating retinal neurogenesis.

NCRNA disease

Although relatively rare worldwide, NCRNA is common in certain geographic areas, and other families have been reported with this disease[16],[17]. Clinically related malformations, such as retinal dysplasia, congenital falciform folds and PHPV, have been described histologically, and may coexist with retinal nonattachment in the same pedigree or contralateral eye. To our knowledge, optic nerve aplasia has not been previously associated with retinal nonattachment. Our findings provide a basis for molecular genetic analysis of these disorders and carrier detection in the Khorasani pedigree.

Coupled neurovascular development in the retina

The ocular pathology in NCRNA patients resembles the phenotype of *Atoh7* mutant mice beyond the absence of optic nerves. In normal mice, retinal vascular development occurs between birth and P14, with spreading of surface vessels from the central artery to the ora serrata, elaboration of two deep vascular plexi, and coordinated regression of the fetal hyaloid network[12]. In *Atoh7* mutants, there is complete agenesis of the intrinsic retinal vasculature[26]. Instead, the fetal vessels persist after birth and collapse upon the retinal surface, where they penetrate and ramify in an irregular pattern. These abnormal vessels are perfused by cilioretinal arteries and the remnant hyaloid trunk, and are prone to hemorrhage. A comparable but less severe neovascularization has been noted in *Bst*/+ mice and some human sporadic optic nerve aplasia cases[34], and may reflect a general deficiency of RGC paracrine factors that control retinal angiogenesis.

In NCRNA patients, the pathogenic sequence of events is likely to be similar to that in *Atoh7* mutant mice, except that the persistent fetal blood vessels appear to proliferate more dramatically during infancy, causing complete perinatal detachment of the retina. This may occur during or shortly after neurogenesis, since the pathology is apparent at birth, and it may have a tractional basis, involving fibrovascular strands between the retina, posterior lens and hyaloid vessels. Indeed, vascular traction is thought to underlie the prevalence of juvenile detachments in patients with ROP, PHPV and FEVR. RGC axons comprising the nerve fiber layer may also stabilize the retina mechanically. The difference between mouse *Atoh7* and human NCRNA phenotypes may reflect the large disparity in scale between species for several parameters: [1] the size of the eye globe compared to the fixed distance for O_2 diffusion and thickness of the neuroretinal shell; [2] the relative volume of the lens and vitreous chamber; [3] the exposure of the retina to mechanical forces; and [4] the surface area requiring perfusion. Consequently, the hypoxia experienced by cells in the newborn retina, and the extent of the proliferative neovascular response, may be significantly greater in NCRNA patients compared to *Atoh7* mutant mice, and this may promote retinal detachment. There are also important differences in retinal structure and timing of vascular development between humans and mice, which may affect NCRNA pathogenesis[13].

Regardless of these differences, the vascular phenotype in both species is a secondary consequence of the absence of RGCs, since *Atoh7* expression is limited to neurons. Although the molecular pathways are not fully defined, ganglion cells are known to stimulate migration of retinal astrocytes from the optic stalk, which promotes the normal program of vascularization[12]. These events are mediated by signaling factors such as Shh, Pdgfa, Vegf and Ndp[2]. In this way, the pathogenesis of NCRNA further highlights the interdependence between neural and vascular development.

The profusion of vitreal blood vessels in NCRNA resembles the vascular events in retinopathy of prematurity, a major form of childhood blindness[35]. Although multiple risk factors have been identified, ROP is primarily stimulated by retinal ischemia during postnatal development, with an excessive angiogenic response. The new vessels create a fibrovascular ridge, near the equator of the globe, with a risk of folding and tractional detachment. The time course for retrolental fibroplasia in NCRNA and ROP progression are similar[18],[36].

In children and adults with NCRNA, recurrent intravitreal hemorrhages may communicate with the anterior chamber, causing chronic corneal blood staining, a local hemosiderin reaction. Although this effect has not been demonstrated histologically in *Atoh7* mutants, hyphemas do occur in these mice[26].

Conserved role for *ATOH7* in retinogenesis

The role of *atonal* bHLH proteins in generating the first retinal neurons has been conserved during vertebrate and invertebrate evolution[5],[37]. In the *Drosophila* eye imaginal disc, Atonal specifies R8 cells, which induce formation of photoreceptors R1–R7 through a succession of cell-cell interactions. Consequently, in *ato* mutant flies, all of these dependent cell types are missing. In *Atoh7* mutant mice and *lakritz* zebrafish, the absence of ganglion cells does not

trigger a similar neurogenic catastrophe. However, the loss of RGC inductive signals does cause a major retinovascular failure in humans with NCRNA disease.

The signals that initiate retinal neurogenesis converge upon *Atoh7* transcriptional enhancers. Several extrinsic factors have been implicated, which may stimulate (FGF), suppress (GDF11) or modulate (SHH) *Atoh7* expression (Supplementary Notes). Likewise, a variety of homeodomain and bHLH proteins appear to act directly upstream, including Pax6 and Neurog2[3],[32],[38]. Functional binding sites have been identified within the bipartite 1.8 kb primary enhancer for mouse, *Xenopus* and chicken *Atoh7*[30]–[32],[39] and are predicted in the most conserved portions of the remote enhancer (Supplementary Fig. 7d,e). These two DNA segments drive expression in the developing retinas of multiple species in an appropriate spatiotemporal pattern for *Atoh7*, despite differences in timing with respect to cell cycle exit. Mouse *Atoh7* is expressed after terminal M phase[4], whereas zebrafish *ath5* is activated during G2 phase of the last cell division, such that every *ath5+* cell gives rise to two daughters[33] (Supplementary Fig. 9d,e). In each case, regulatory protein complexes are likely to assemble on the enhancer chromatin in mitotic progenitors prior to *Atoh7* transcription, in a latent configuration, defining the RGC competence state[1]. The factors that mark these cells for terminal division are unknown.

The shadow enhancer and optic nerve development

On the basis of our findings, we speculate that the remote CNEs may function as a 'shadow' or *secondary* enhancer for *ATOH7*. This class of regulatory elements are thought to reinforce, refine or stabilize the effects of *primary* enhancers and may serve as vehicles for evolutionary change[21],[40]. First, the NCRNA element is located ~20kb from the primary *ATOH7* enhancer, which is close to the mRNA initiation site, and therefore presumably interacts with the promoter during retinogenesis via chromatin looping (Supplementary Fig. 10). Second, the remote and primary enhancers drive nearly identical patterns of expression, and are thus at least partly redundant (Fig. 7). The two enhancers have no obvious sequence similarity, suggesting an independent evolutionary origin, and may have different selective constraints. They appear to have evolved as separate entities in the tetrapod lineage, by progressive displacement of 5′ regulatory modules from a single ancestral cluster (Supplementary Fig. 7c) with refinement by accumulation of point mutations. Third, the remote enhancer may be important for evolutionary fitness.

Why does *ATOH7* have duplicate enhancers? Each is sufficient for appropriate reporter expression in transgenic mice and, although not formally tested, both are likely to be necessary for full development of RGCs *in vivo*. The remote enhancer may greatly boost the level of gene expression, acting via a cooperative mechanism, or stabilize the onset of transcription at a critical early stage of retinal histogenesis. In principle, delayed development of RGCs, due to a disruption in *Atoh7* expression or cellular metabolism, could prevent ganglion cell axons from exiting the optic cup before closure of the choroid fissure, leading to optic nerve hypoplasia and/or coloboma. These effects may be compounded because retinal neurogenesis in some vertebrates appears to propagate as a wave, suggesting a feed-forward mechanism. This may involve direct binding of Atoh7 protein to E-box sites in the proximal enhancer[32], although there is no evidence for *Atoh7* autoregulation in

mammals[5]. Alternatively, an internal neurogenic timer may be cued by a gradient of signaling molecules[41]. In either model, dual enhancers would assure robust firing of *Atoh7* transcripts.

Congenital optic nerve malformations are relatively common causes of severe visual impairment in humans and have environmental and genetic risk factors. Optic nerve hypoplasia (ONH) affects 12% of blind children and often occurs with hypothalamic, pituitary or other CNS abnormalities (Supplementary Notes). Mutations in several genes are known to cause ONH in humans or mice, including *Pax6*, *Pou4f2*, *Rx*, *Hesx1*, *Otx2*, *Six6, Chx10*, *Sox2*, *Dcc*, *Ntn1* and *Rpl24*. Bilateral optic nerve aplasia is the most extreme ocular manifestation of this disease spectrum. There is also considerable variation in optic disc size among healthy people[42] and RGC number among inbred strains of mice[43]. In humans, two recent genome-wide association studies (GWAS) implicate the *ATOH7* region as the most important determinant of variation in optic disc area, which is directly related to RGC number[44,45]. Remarkably, the highest statistical significance for this papillometric trait is centered over the NCRNA deletion, including one genotyped SNP (rs3858145) in the shadow enhancer (Fig. 3c, Supplementary Fig. 8b).

The earliest stages of retinal neurogenesis may be relatively precarious, particularly the brief but essential burst of *Atoh7* transcription, which is required for vision and thus evolutionary survival. In this way, the remote enhancer may buffer this critical process against environmental and genetic stresses, as recently demonstrated for the *svb* and *snail* loci in *Drosophila*[46,47]. The dual enhancers appear to function equivalently but have no obvious sequence similarity, apart from short motifs (Supplementary Fig. 7). In future studies, it will be important to identify the molecular factors that activate these enhancers *in vivo*, triggering the onset of retinal histogenesis, and to determine the transcriptional and phenotypic effects of deleting the orthologous remote enhancer in mice.

The NCRNA deletion may silence *ATOH7* expression entirely, as a null allele, or prevent high-level transcription, similar to deletions of the *HBB* locus control region or 3′ *PAX6* enhancer. A gain-of-function mechanism is unlikely, since NCRNA heterozygotes are normal, and transgenic mice with broad ectopic retinal expression of *Atoh7* have no obvious histopathology[48]. Although remote regulatory mutations are known in human genetics, the NCRNA deletion provides a clear example of a Mendelian disease involving a duplicate or 'shadow' enhancer.

MATERIALS AND METHODS

Clinical studies

Detailed eye exams and photography were performed on 12 patients for this study at Emam Ali Hospital in Bojnourd, North Khorasan. In addition, the findings reflect observations from over 40 NCRNA patients examined at regional clinics during the past two decades[18]. Magnetic resonance images (MRI) were obtained for an 18 year-old male subject in Tehran, using a Siemens Magnetom Expert-plus instrument. The orbital MRI protocol included T1W SE-90, T2 TIR-180, T1 TSE-180 and T1 SE sequences, with fat suppression, before and after administration of gadolinium contrast. Images were collected in horizontal, coronal and

oblique sagittal planes. Approval was obtained from Shahid Beheshti University Medical School and University of Michigan institutional review boards in accordance with accepted guidelines.

Mutation screening

Genomic DNA samples from 150 pedigree members were collected as part of a previous linkage study[19] and include 28 blind subjects. We amplified 184 exonic and 25 intergenic fragments from the 14 positional candidates by PCR using custom oligonucleotide primers (Supplementary Tables 1–3, Supplementary Fig. 1) and a 2:1 mixture of Platinum *Taq* (Invitrogen) and EXPAND Hi-Fidelity (Roche) polymerases. Segments spanning the GC-rich *ATOH7* gene and 5′ flanking DNA were amplified in the presence of betaine[29] as detailed (Supplementary Table 1). Screening was performed on a core panel of samples from blind (rr), obligate carrier (Rr) and wild-type (RR) individuals. To minimize potential effects of chemical inhibitors and DNA damage, a multiple displacement amplification (MDA) step (Repli-g, Qiagen) was included before PCR. Products were sequenced directly after agarose gel purification (Wizard SV gel system, Promega). Endpoints of the NCRNA deletion were determined by junctional PCR, using five different primer pairs. RR homozygotes and Rr family members were identified based on previous 10q SSLP haplotype analysis[20]. As expected, blind individuals were homozygous for all SNPs surveyed within the nonrecombinant interval.

To determine NCRNA genotypes in family members throughout the pedigree, and identify mutation carriers, we used a triplex PCR strategy. Diagnostic reactions (25μl) were performed in 1X PCR buffer (50 mM KCl, 20 mM Tris pH 8.4, 1.5 mM $MgCl_2$) containing 0.3 M betaine (1X MasterAmp™, Epicentre)[29], 200 μM dNTPs, 0.25 U *Taq* polymerase (Invitrogen), 75 ng genomic DNA and three primers (5 pmol each). The reverse primers were 30R (5′-CCCAGTGTTTCCTAGCTTTGTTAGG) and 37R (5′-TTCAGAACAGGAGCAGCGTG), and the common forward primer was 30F*ref* (5′-TGCAAGGACTTTGTGGCTCTTG). PCRs were performed in a 96-well MJ Thermocycler with the following protocol: 95°C × 5 min; followed by 40 cycles of 95°C denaturation × 45 sec, 55°C annealing × 45 sec, and 72°C extension × 60 sec; followed by a final 72°C extension step for 7 min, with termination at 4°C. Allelic wild-type (727 bp) and NCRNA deletion (462 bp) products were resolved on a 1% agarose gel.

SNP analysis

Four archival samples from the NCRNA pedigree, and fresh blood and lymphoblastoid cell line DNA from one blind (rr) individual, were genotyped for 1.1 million informative SNP (single nucleotide polymorphism) markers, distributed with 2.4 kb average spacing genome-wide, including 390 SNPs in the NCRNA critical interval. Genotypes were determined using the Illumina Omni1-quad Infinium BeadChip platform and analyzed for dosage (logR ratio) and heterozygosity (B allele frequency) using GenomeStudio software.

Reverse transcriptase (RT)-PCR

Total RNA was isolated from adult retina, liver, kidney and heart tissues and E14.5 fetal eyes of C57BL/6 mice by Trizol extraction (Invitrogen) and treated with RNase-free DNase

(Roche). cDNA was generated from 5 μg RNA using $d(N)_6$ random hexamers, recombinant RT (Superscript II, Invitrogen) and RNaseH in a 40 μl reaction, and 1 μl of the resulting cDNA was used as template per 25 μl PCR. Products were amplified for 34 cycles with Platinum *Taq* (Invitrogen) using primers specific for *Atoh7*, *Mypn*, *Pbld* and *Actb* (Supplementary Fig. 3). The PCR cycles were 95°C denaturation × 45 sec, 58°C annealing × 45 sec, and 72°C extension × 60 sec.

Plasmid constructs

Plasmid p3034-BGnCherry was created by inserting a 3834 bp human genomic fragment into the *Xba*I and *Bam*HI sites of pBGnCherry (kindly provided by Jane Johnson), in the normal transcriptional orientation. This vector contains a minimal human β-globin promoter (BG) and a monomeric Cherry red fluorescent protein reporter cassette (nuCherry) with a synthetic amino-terminal nuclear localization signal (MAPKKKRKVEDV) downstream of the *Bam*HI site, and it has no intrinsic activity in transgenic mice. The fragment was amplified from human BAC clone RP24-1114I5 with primers 30F*ref-Spe*I (CATTTAACTaGTCAGCTTGCAAGGACTTTGTGGC) and 34R (5′-GTGAATCAAAGTACAGCATGATGG) and EXPAND Hi-Fidelity polymerase, creating a terminal *Spe*I restriction site. The fragment was purified after digestion with *Spe*I and *Bam*HI, subcloned, and verified by sequencing. It extends between −21.9 kb and −18.1 kb, relative to the *ATOH7* transcription start site (TSS), and spans three CNEs within the NCRNA deletion.

Transgenic mice

Founder embryos and one stable transgenic line were generated by injecting the 5.0 kb *Sal*I-*Psp*OMI fragment of plasmid p3034-BGnCherry into fertilized (C57 x SJL) F2 or (B6SJL × CD-1 *Atoh7*[tm1Gla]) F1 oocytes. To directly compare nuCherry and *Math5-lacZ* expression, we examined embryos carrying the *Atoh7*[tm1Gla] *lacZ* knock-in allele[5]. Math5-GFP mice carry an EGFP reporter transgene regulated by a 2.1 kb mouse DNA segment that contains the *Atoh7* promoter, 5′UTR and 1.8 kb upstream genomic DNA[49],[31]. Embryos from timed pregnancies were evaluated for nuCherry and GFP expression by stereofluorescence microscopy, or were fixed in 4% paraformaldehyde (PFA), cryosectioned and immunostained. To assess cell division, gravid dams were given an intraperitoneal injection of BrdU (100 mg/kg) one hour before harvest. Wholemount GFP and nuCherry images were obtained using 480/40 or 560/40 nm excitation, and 510 or 610 nm LP emission filters, respectively, with a Leica MZ FLIII stereomicroscope.

Immunostaining

Fixed sections or dissociated cells were blocked with 0.5% Triton X-100, 0.1 M $NaPO_4$ pH 7.3 (PBTx) with 1% bovine serum albumin (BSA) and 10% normal donkey serum (NDS). Primary antibodies were applied overnight at 4°C in PBTx with 3% NDS 1% BSA. After washing in PBS 0.5% BSA, minimally cross-reactive donkey anti-rabbit IgG sera conjugated with biotin (1:500), or donkey anti-chicken IgY or anti-rat IgG sera conjugated with Dylight-488 (1:1000, Jackson Immunoresearch, West Grove, PA), was applied for 2 hr at room temperature. After secondary antibody staining and washing in PBS 0.5% BSA,

tertiary streptavidin-conjugated Texas Red (1:400) or Dylight-594 (1:1000) reagents were applied for 1 hr in PBTx with 1 μg/ml 4′,6-diamidino-2- phenylindole (DAPI). Slides were then washed in PBS and visualized by epifluorescence (Olympus BX-51) or laser confocal microscopy (Zeiss LSM-510). Primary antibodies were anti-DsRed (Clontech rabbit polyclonal, 1:500) for *Discoma sp.* nuCherry; anti-GFP (Abcam chicken polyclonal, 1:2000); anti-β-galactosidase (rat polyclonal, 1:1000); and anti-BrdU (Harlan BU/175 rat monoclonal, 1:100). Genetic and serologic controls showed no cross-detection of nuCherry and GFP antigens. BrdU immunostaining was performed as a terminal procedure, following application of other 1° and 2° antibodies and an antigen retrieval step (2.4 N HCl in PBS 0.4% Triton X-100 for 1 hr). PH3 (phosphohistone H3) was detected using polyclonal rabbit antibody directly conjugated to Alexa-448 (Cell Signaling 9708, 1:50), after nuCherry immunostaining and 10% normal rabbit serum blocking steps, or a mouse monoclonal (6G3, Cell Signaling, 1:100) with biotinylated anti-mouse IgG and Alexa-647 streptavidin.

Flow cytometry

Double-positive E14.5 littermates carrying nuCherry and GFP reporters were generated, along with single-positive and double-negative controls, by crossing Math5-GFP and 3034-BGnCherry transgenic mice. Genotypes were provisionally assigned by retinal fluorescence and verified by PCR of amniotic membrane DNA. Neural retinas from each embryo were dissected in cold PBS and dissociated by digestion with 1 μg/ml trypsin (Gibco) for 15 min at 37°C, with intermittant trituration, in a 400 μl volume. The reaction was terminated by addition of 1 μg/ml SBTI (soybean trypsin inhibitor, igma), 2.5 mM $MgCl_2$ and 100 μg/ml DNase I (Sigma). Freshly dissociated cells were kept on ice, protected from light, and sieved immediately prior to flow cytometric analysis by centrifugation at $100 \times g$ for 5 min into 70 μm mesh strainer collection tubes (BD Biosciences).

Two-dimensional flow cytometry was performed using a BD FACS Diva instrument equipped with 488 nm argon and 561 nm solid-state excitation lasers (Spectraphysics) and 510/21 nm and 610/20 nm bandpass emission filters (Omega optics) to detect GFP and nuCherry fluorescence, respectively. No spectral compensation was required. Two embryos of each genotype ($n = 8$) were analyzed. For each cell suspension, the primary population was gated using FSC-A (forward scatter) and SSC-A (side scatter), and multiparticle events were excluded using the FSC-W parameter. Living cells (95%) were further gated by DAPI (1 μg/ml) exclusion, which was detected using a 351 nm UV laser (Coherent 300) and 424/44 nm bandpass filter. Flow data from 10,000 events were analyzed for each embryo using BD FACS Diva software.

To visualize dissociated retinal cells, 20 μl aliquots from each suspension were plated on 8-well chamber glass slides coated with poly-D-lysine, and the adherent cells were fixed with 4% PFA. Immunocytochemistry was performed as noted above, with rabbit anti-DsRed (1:2000) and chicken anti-GFP (1:5000). Cells were viewed using an Olympus BX-51 microscope with widefield fluorescence optics and a 100X oil immersion objective.

Transgenic fish

Zebrafish in our breeding colony originated from a local pet store and are maintained at 28°C with a 10/14 hour light/dark cycle. Transgenic fish were produced by *Tol2* transposase-mediated integration (Supplementary Notes). Expression cassettes (*3034-BGnCherry* and *BGnCherry* control) were subcloned between the *Xho*I and *Bsr*GI sites of pT2AL200R150G, a plasmid vector that harbors *Tol2* transposable elements flanking the cloning site. Capped *Tol2* transposase mRNA was synthesized from *Not*I-linearized pCS-TP template using the Mmessage Mmachine SP6 kit (Ambion), purified by phenol-chloroform extraction, precipitated with isopropanol, and resuspended in nuclease-free water at 1 μg/ml. Approximately 0.3 μl of a mixture containing 25 ng/μl supercoiled expression plasmid DNA and 25 ng/μl *Tol2* transposase mRNA was injected into fertilized zebrafish eggs at the 1–2 cell stage. Injected embryos were surveyed for nuCherry expression 2–5 days post-fertilization (dpf) using a Leica MZ FLIII stereofluorescence microscope. No expression was detected in embryos injected with the control *BGnCherry* construct, whereas most embryos injected with the *3034-BGnCherry* exhibited bright red fluorescence. Approximately 100 embryos expressing the reporter were grown to adulthood.

To identify germline integration of the transgene, injected fish were bred in groups of 6–8, and their offspring were examined for nuCherry expression. Groups containing fluorescent progeny were outcrossed to identify founders (F_0) with transgenes integrated in the germline. The resulting N_1 progeny were then bred to wild- type fish to perpetuate heterozygous lines harboring solitary transgenes flanked by LTRs. Three *3034-BGnCherry* lines were generated in this way. To visualize retinal nuCherry expression in transparent embryos, 0.003% 1-phenyl-2-thiourea (PTU) was added to the water at 12 hpf to inhibit pigment formation. *3034-BGnCherry* progeny were also crossed to the *ath5:GFP* line (kindly provided by Ichiro Masai), which carries a GFP transgene regulated by 7 kb genomic DNA from zebrafish *ath5* (Supplementary Notes). Mitotic cells were labeled by immersing zebrafish embryos for 20 min in 1 mM EdU (ethynyl deoxyuridine) 15% DMSO prior to fixation in 4% PFA and cryopreservation. EdU-labeled nuclei were detected using $CuSO_4$ and Alexafluor 647 azide (Click-iT reagents, Invitrogen).

Informatics

Sequence comparisons were performed between remote and primary *ATOH7* enhancer elements in human and mouse genomes using pairwise BLAST (http:// blast.ncbi.nlm.nih.gov/Blast.cgi). Upstream *ATOH7* regulatory regions from diverse taxa were aligned using pairwise (BLASTZ), MultiZ and PhastCons features of the UCSC browser (http://genome.ucsc.edu), for panels containing 12 eutherian mammals and 37 vertebrate species (Supplementary notes) and mVISTA (LAGAN). To search for homologous amphibian and fish sequences, we interrogated *Xenopus*, teleost (*Danio*, *Oryzias*, *Gasterosteus*, *Tetraodon*) and lamprey (*Petromyzon*) genomes and upstream regions with individual CNE segments from the NCRNA deletion, using high- and low-stringency search parameters. PCR sequence analysis and optimal primer design for mutation screening were performed using MacVector 7.2 software (Accelrys). For mutation screening, PCR sequences from the NCRNA pedigree were compared to the NCBI reference genome (NCBI36/hg18, Mar 2006 assembly) and known variants (dbSNP, including the

March 2010 interim release from the *1000 genomes* project). Potential regulatory motifs for DNA-binding factors were identified using multiple analysis tools, including the JASPAR database (http://jaspar.genereg.net/).

Supplementary Material

Refer to Web version on PubMed Central for supplementary material.

Acknowledgments

References

1. Livesey FJ, Cepko CL. Vertebrate neural cell-fate determination: lessons from the retina. Nat Rev Neurosci. 2001; 2:109–118. [PubMed: 11252990]

2. West H, Richardson WD, Fruttiger M. Stabilization of the retinal vascular network by reciprocal feedback between blood vessels and astrocytes. Development. 2005; 132:1855–1862. [PubMed: 15790963]

3. Brown NL, et al. Math5 encodes a murine basic helix-loop-helix transcription factor expressed during early stages of retinal neurogenesis. Development. 1998; 125:4821–4833. [PubMed: 9806930]

4. Brzezinski JA, Glaser T. Math5 establishes retinal ganglion cell competence in postmitotic progenitor cells. Invest Ophthalmol Vis Sci. 2004; 45:3422. E-abstract.

5. Brown NL, Patel S, Brzezinski J, Glaser T. Math5 is required for retinal ganglion cell and optic nerve formation. Development. 2001; 128:2497–2508. [PubMed: 11493566]

6. Wang SW, et al. Requirement for math5 in the development of retinal ganglion cells. Genes Dev. 2001; 15:24–29. [PubMed: 11156601]

7. Brzezinski JA, et al. Loss of circadian photoentrainment and abnormal retinal electrophysiology in Math5 mutant mice. Invest Ophthalmol Vis Sci. 2005; 46:2540–2551. [PubMed: 15980246]

8. Kay JN, Finger-Baier KC, Roeser T, Staub W, Baier H. Retinal ganglion cell genesis requires lakritz, a Zebrafish atonal Homolog. Neuron. 2001; 30:725–736. [PubMed: 11430806]

9. Yang Z, Ding K, Pan L, Deng M, Gan L. Math5 determines the competence state of retinal ganglion cell progenitors. Dev Biol. 2003; 264:240–254. [PubMed: 14623245]

10. Mu X, et al. A gene network downstream of transcription factor Math5 regulates retinal progenitor cell competence and ganglion cell fate. Dev Biol. 2005; 280:467–481. [PubMed: 15882586]

11. Gariano RF, Gardner TW. Retinal angiogenesis in development and disease. Nature. 2005; 438:960–966. [PubMed: 16355161]

12. Fruttiger M. Development of the retinal vasculature. Angiogenesis. 2007; 10:77–88. [PubMed: 17322966]

13. Provis JM. Development of the primate retinal vasculature. Prog Retin Eye Res. 2001; 20:799–821. [PubMed: 11587918]

14. Wright AF, Chakarova CF, Abd El-Aziz MM, Bhattacharya SS. Photoreceptor degeneration: genetic and mechanistic dissection of a complex trait. Nat Rev Genet. 2010; 11:273–284. [PubMed: 20212494]

15. Swaroop A, Kim D, Forrest D. Transcriptional regulation of photoreceptor development and homeostasis in the mammalian retina. Nat Rev Neurosci. 2010; 11:563–576. [PubMed: 20648062]

16. Warburg M. Retinal malformations: aetiological heterogeneity and morphological similarity in congenital retinal non-attachment and falciform folds. Doyne Memorial Lecture. Trans Ophthalmol Soc U K. 1979; 99:272–283. [PubMed: 298427]

17. Phillips CI, Stokoe NL. Congenital hereditary bilateral nonattachment of retina: a sibship of two males. J Pediatr Ophthalmol Strabismus. 1979; 16:358–363. [PubMed: 521877]

18. Ghiasvand NM, Shirzad E, Naghavi M, Vaez Mahdavi MR. High incidence of autosomal recessive nonsyndromal congenital retinal nonattachment (NCRNA) in an Iranian founding population. Am J Med Genet. 1998; 78:226–232. [PubMed: 9677055]

19. Ghiasvand NM, et al. Nonsyndromic congenital retinal nonattachment gene maps to human chromosome band 10q21. Am J Med Genet. 2000; 90:165–168. [PubMed: 10607958]

20. Ghiasvand NM, Fleming TP, Helms C, Avisa A, Donis-Keller H. Genetic fine mapping of the gene for nonsyndromic congenital retinal nonattachment. Am J Med Genet. 2000; 92:220–223. [PubMed: 10817658]

21. Hong JW, Hendrix DA, Levine MS. Shadow enhancers as a source of evolutionary novelty. Science. 2008; 321:1314. [PubMed: 18772429]

22. Perry JR. Forced migration in Iran during the seventeenth and eighteenth centuries. Iranian Studies. 1975; 8:199–215.

23. Brodrick JD. Corneal blood staining after hyphaema. Br J Ophthalmol. 1972; 56:589–593. [PubMed: 5079405]

24. Brodsky, MC. Paediatric Neuro-ophthalmology. Springer; New York: 2010. Nystagmus in children; p. 383-442.

25. Van Gelder RN, Wee R, Lee JA, Tu DC. Reduced pupillary light responses in mice lacking cryptochromes. Science. 2003; 299:222. [PubMed: 12522242]

26. Brzezinski JA, et al. Retinal ganglion cells are required for normal retinal vascular development and hyaloid regression. Dev Biol. 2011 in press.

27. Lin B, Wang SW, Masland RH. Retinal ganglion cell type, size, and spacing can be specified independent of homotypic dendritic contacts. Neuron. 2004; 43:475–485. [PubMed: 15312647]

28. Brown NL, Dagenais SL, Chen CM, Glaser T. Molecular characterization and mapping of ATOH7, a human atonal homolog with a predicted role in retinal ganglion cell development. Mamm Genome. 2002; 13:95–101. [PubMed: 11889557]

29. Prasov L, Brown NL, Glaser T. A critical analysis of Atoh7 (Math5) mRNA splicing in the developing mouse retina. PLoS ONE. 2010; 5:e12315. [PubMed: 20808762]

30. Hutcheson DA, et al. bHLH-dependent and -independent modes of Ath5 gene regulation during retinal development. Development. 2005; 132:829–839. [PubMed: 15677728]

31. Riesenberg AN, et al. Pax6 regulation of Math5 during mouse retinal neurogenesis. Genesis. 2009; 47:175–187. [PubMed: 19208436]

32. Skowronska-Krawczyk D, et al. Conserved regulatory sequences in Atoh7 mediate nonconserved regulatory responses in retina ontogenesis. Development. 2009; 136:3767–3777. [PubMed: 19855019]

33. Poggi L, Vitorino M, Masai I, Harris WA. Influences on neural lineage and mode of division in the zebrafish retina in vivo. J Cell Biol. 2005; 171:991–999. [PubMed: 16365165]

34. Lee BL, Bateman JB, Schwartz SD. Posterior segment neovascularization associated with optic nerve aplasia. Am J Ophthalmol. 1996; 122:131–133. [PubMed: 8659592]

35. Chen J, Smith LE. Retinopathy of prematurity. Angiogenesis. 2007; 10:133–140. [PubMed: 17332988]

36. Palmer EA, et al. Incidence and early course of retinopathy of prematurity. The Cryotherapy for Retinopathy of Prematurity Cooperative Group. Ophthalmology. 1991; 98:1628–1640. [PubMed: 1800923]

37. Hsiung F, Moses K. Retinal development in Drosophila: specifying the first neuron. Hum Mol Genet. 2002; 11:1207–1214. [PubMed: 12015280]

38. Hufnagel RB, Le TT, Riesenberg AL, Brown NL. Neurog2 controls the leading edge of neurogenesis in the mammalian retina. Dev Biol. 2009; 340:490–503. [PubMed: 20144606]

39. Willardsen MI, et al. Temporal regulation of Ath5 gene expression during eye development. Dev Biol. 2009; 326:471–481. [PubMed: 19059393]

40. Hobert O. Gene regulation: enhancers stepping out of the shadow. Curr Biol. 2010; 20:R697–699. [PubMed: 20833307]

41. Kay JN, Link BA, Baier H. Staggered cell-intrinsic timing of ath5 expression underlies the wave of ganglion cell neurogenesis in the zebrafish retina. Development. 2005; 132:2573–2585. [PubMed: 15857917]

42. Hoffmann EM, Zangwill LM, Crowston JG, Weinreb RN. Optic disk size and glaucoma. Surv Ophthalmol. 2007; 52:32–49. [PubMed: 17212989]

43. Williams RW, Strom RC, Goldowitz D. Natural variation in neuron number in mice is linked to a major quantitative trait locus on Chr 11. J Neurosci. 1998; 18:138–146. [PubMed: 9412494]

44. Macgregor S, et al. Genome-wide association identifies ATOH7 as a major gene determining human optic disc size. Hum Mol Genet. 2010; 19:2716–2724. [PubMed: 20395239]

45. Ramdas WD, et al. A genome-wide association study of optic disc parameters. PLoS genetics. 2010; 6:e1000978. [PubMed: 20548946]

46. Frankel N, et al. Phenotypic robustness conferred by apparently redundant transcriptional enhancers. Nature. 2010; 466:490–493. [PubMed: 20512118]

47. Perry MW, Boettiger AN, Bothma JP, Levine M. Shadow enhancers foster robustness of Drosophila gastrulation. Curr Biol. 2010; 20:1562–1567. [PubMed: 20797865]

48. Prasov L, Glaser T. Math5 confers multipotency in fate-restricted post-mitotic retinal precursors. Invest Ophthal Vis Sci. 2009; 50:1310. E-abstract.

49. Hufnagel RB, Riesenberg AN, Saul SM, Brown NL. Conserved regulation of Math5 and Math1 revealed by Math5-GFP transgenes. Mol Cell Neurosci. 2007; 36:435–448. [PubMed: 17900924]
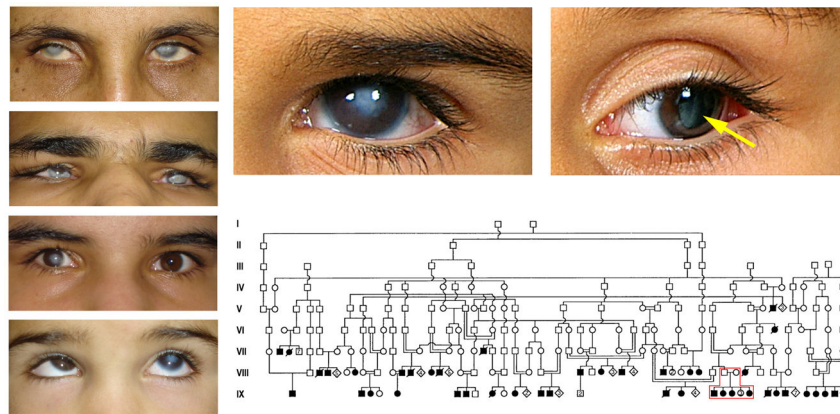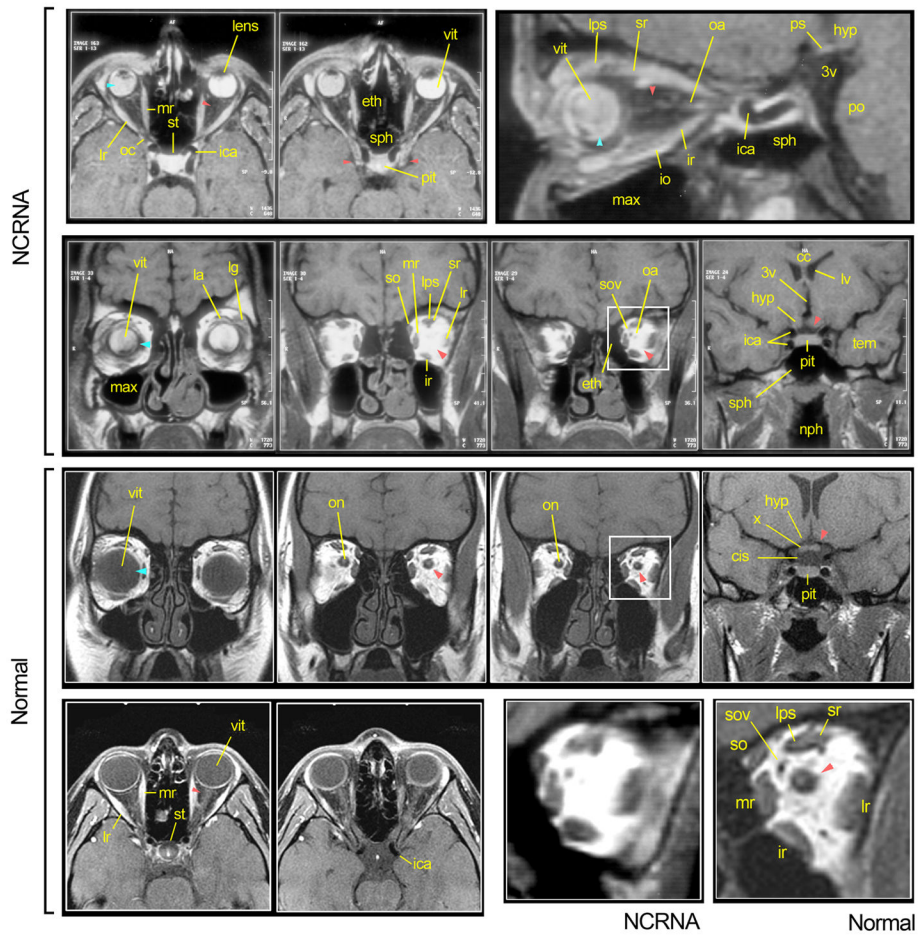
Figure 1.

NCRNA disease. **A–F.** Eye photographs from NCRNA family. **A.** 49-yr old female **B.** 18-yr old male **C.** 14-yr old female **D.** 8-yr old male. Retinal detachments are evident as leukocoria (white pupils) in each case. The NCRNA patients eventually develop dense gray posterior corneal opacities, consistent with chronic blood staining (**A**, **B**, patient's right eye in **C**). They typically exhibit nystagmus and strabismus (esotropia, **D**). The pupils are round, but do not react to light. **E–F.** Closer views showing leukocoria in young patients prior to corneal opacification. **E.** 5-yr old male (left eye). **F.** 3-yr old male (left eye). The detached retina and fibrovascular mass are visible behind the clear lens (arrow). **G.** Khorasani pedigree showing autosomal recessive inheritance of the disease over nine generations, with index cases used for mutation screening (red boxes).
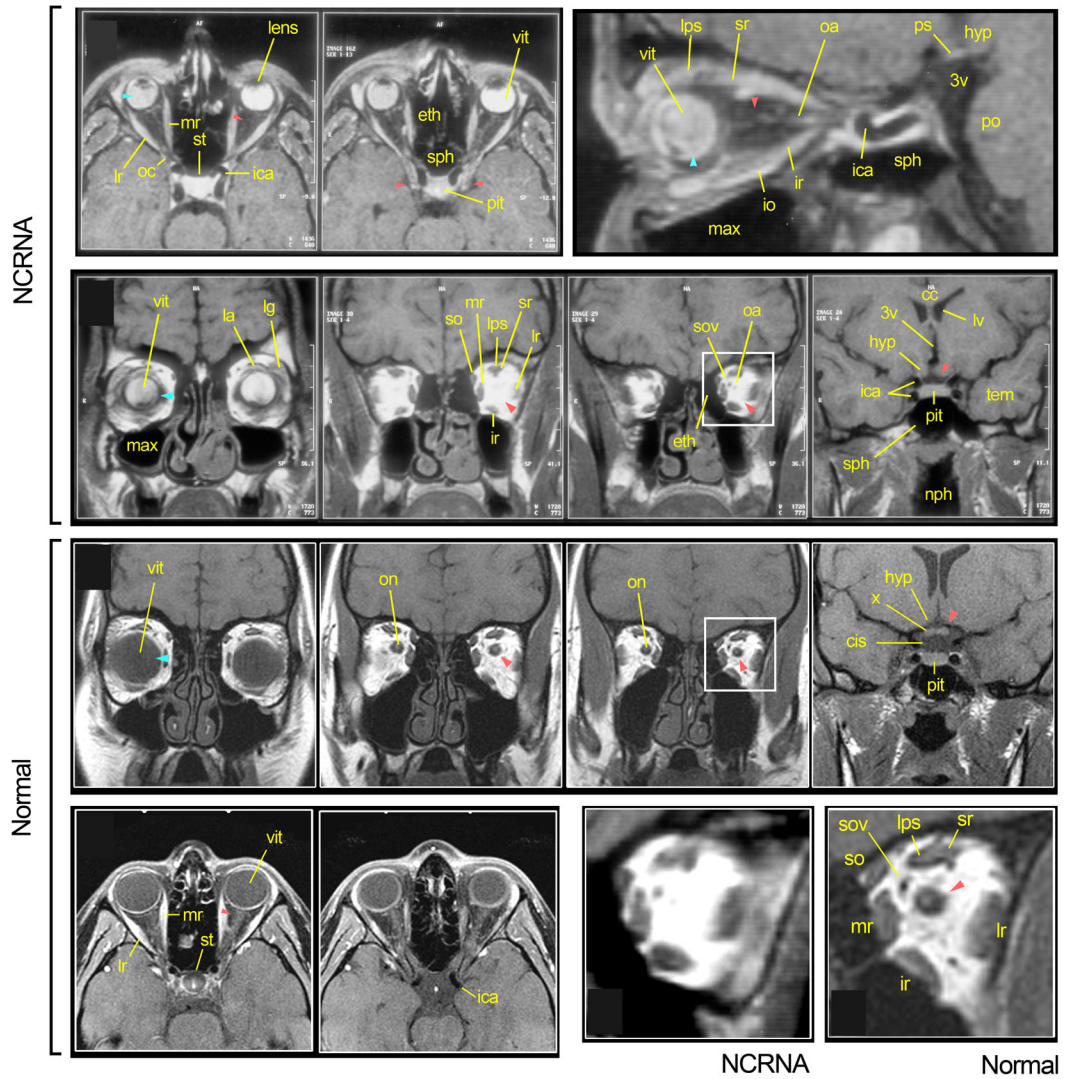
Figure 2.
Anatomical findings in NCRNA. **A–C.** Orbital magnetic resonance images (MRI) of an 18-yr old male patient, showing absence or severe atrophy of the optic nerves and chiasm (red arrowheads), and bilateral detached retinas with vitreous consolidation (bright signal, blue arrowheads). **A.** Axial (TR/TE = 780/15 ms, 3 mm slices) and **B.** Oblique sagittal (right eye, TR/TE = 730/15 ms, 2 mm slice) T1-weighted SE views, with fat suppression and gadolinium contrast. **C.** Coronal T1-weighted SE views (TR/TE = 780/15, 5 mm slices) with no contrast or fat suppression, shown from anterior (left) to posterior (right). **D.** Matched coronal images from a normal 15-yr old female. T1-weighted SE views (TR/TE = 550/11 ms, 3 mm slices). The vitreae are clear (left panel, dark signal, blue arrowhead) and the optic nerves are prominent (middle panels, red arrowheads). The optic chiasm is visible above the suprasellar cistern and pituitary (right panel, red arrowhead). **E.** Matched axial images from the normal subject (TR/TE = 750/11 ms, 3 mm slices). **F,G.** Enlarged coronal views of NCRNA and normal subjects (left orbits, boxed areas in panels C and D). The red arrowhead shows the normal optic nerve. The bright T1W signal outlining the optic nerve,

extraocular muscles (sr, lr, ir, mr, so, lps) and blood vessels (sov) originates from retrobulbar fat. 3v, third ventricle; cc, corpus callosum; cis, suprasellar cistern; eth, ethmoid sinus; hyp, hypothalamus; ica, internal carotid artery; io, inferior oblique; ir, inferior rectus; la, levator aponeurosis; lg, lacrimal gland; lps, levator palpebrae superioris; lr, lateral rectus; lv, lateral ventricle; max, maxillary sinus; mr, medial rectus; nph, nasopharynx; oa, ophthalmic artery; oc, optic canal; on, optic nerve; pit, pituitary gland; po, pons; ps, pituitary stalk; so, superior oblique; sov, superior orbital vein; sph, sphenoid sinus; sr, superior rectus; st, sella turcica; tem, temporal lobe; vit, vitreous; x, optic chiasm.
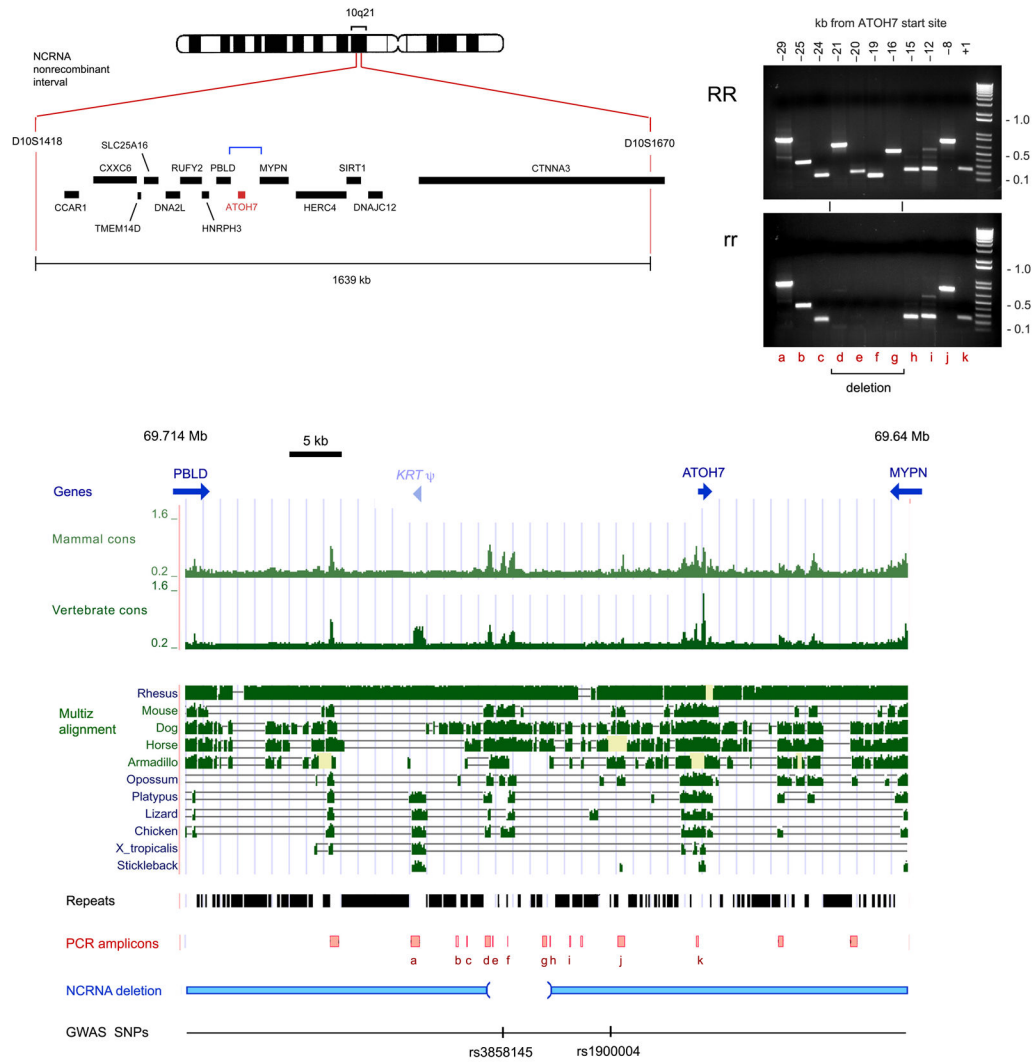
Figure 3.
Homozygous deletion of 5′ *ATOH7* genomic sequences in NCRNA patients. **A.** The 1639 kb critical region on chromosome 10q21 spans 14 positional candidate genes. The segment between *PBLD* to *MYPN* (blue bracket) is expanded below. **B.** Genomic PCRs showing deletion of four adjacent amplicons in an NCRNA patient. Two additional amplicons were also missing (Supplementary Table 3). **C.** Map of 74 kb intergenic region surrounding *ATOH7* (Chr10:69,714,052–69,640,048) modified from the UCSC browser (NCBI36/hg18, Mar 2006 assembly), showing the terminal exons of flanking genes; *KRTψ* (human-specific keratin-18 pseudogene); vertebrate and mammalian evolutionary conservation tracks (PhastCons); interspersed repetitive elements; PCR amplicons (red) used to compare homozygous mutant (rr) and wild-type (RR) DNA samples; and the 6.5 kb NCRNA deletion. Orthologous vertebrate sequences are indicated in the vertebrate MultiZ alignment. In the nontherian genomes, similarity between *KRTψ* and unlinked keratin loci gives a false positive signal of homologous evolution. The corresponding mouse *Pbld-Mypn* intergenic segment is 42.5 kb. Two SNPs (single nucleotide polymorphisms) associated with optic disc area in human genome-wide studies[44],[45] are indicated for comparison (rs1900004,

rs3858145). The deletion removes a cluster of CNEs (conserved noncoding elements) ~20 kb upstream of *ATOH7*.
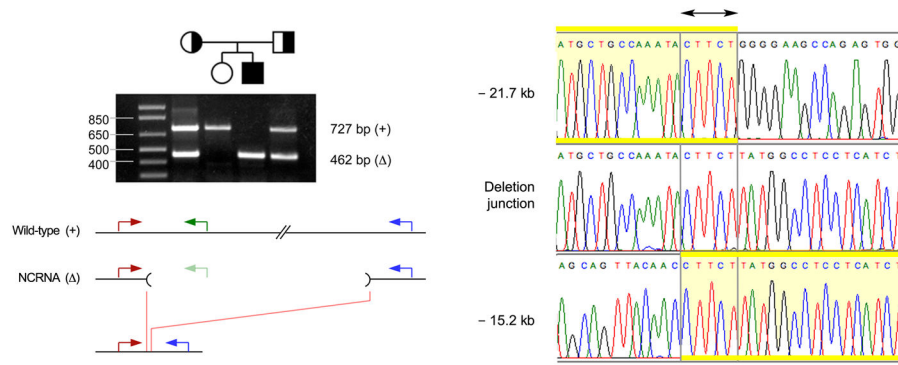
Figure 4.
Endpoints of the NCRNA deletion. **A.** Triplex PCR genotypes showing transmission of the mutation in a small family. **B.** Sequence chromatograms from PCR products showing the distal and proximal breakpoints in wild-type DNA, with 5 bp microhomology (double arrow), and the deletion junction in a DNA from a blind individual.
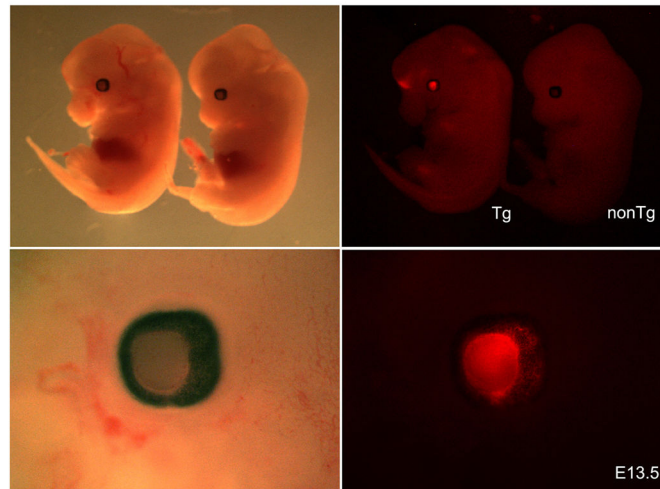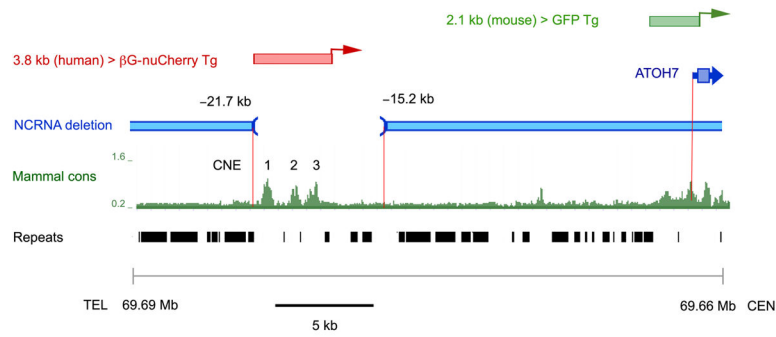
Figure 5.
The NCRNA mutation deletes an *ATOH7* retinal enhancer. **A.** Map of the 30kb upstream region (Chr10:69,690,000–69,660,000) modified from the UCSC browser (NCBI36/hg18, Mar 2006 assembly), showing mammalian basewise sequence conservation and the NCRNA deletion. The 3034-BGnCherry transgene contains 3.8 kb human genomic DNA, which spans the three deleted CNEs and regulates expression from the minimal human β-globin promoter. The location of the Math5-GFP transgene is shown for comparison. This reporter contains the endogenous mouse *Atoh7* promoter, 0.3 kb 5′UTR and 1.8 kb upstream genomic DNA[31]. **B–E.** Brightfield (**B,C**) and fluorescence (**D,E**) images show eye-specific nuCherry expression in a pigmented E13.5 transgenic founder. Tg, transgenic.
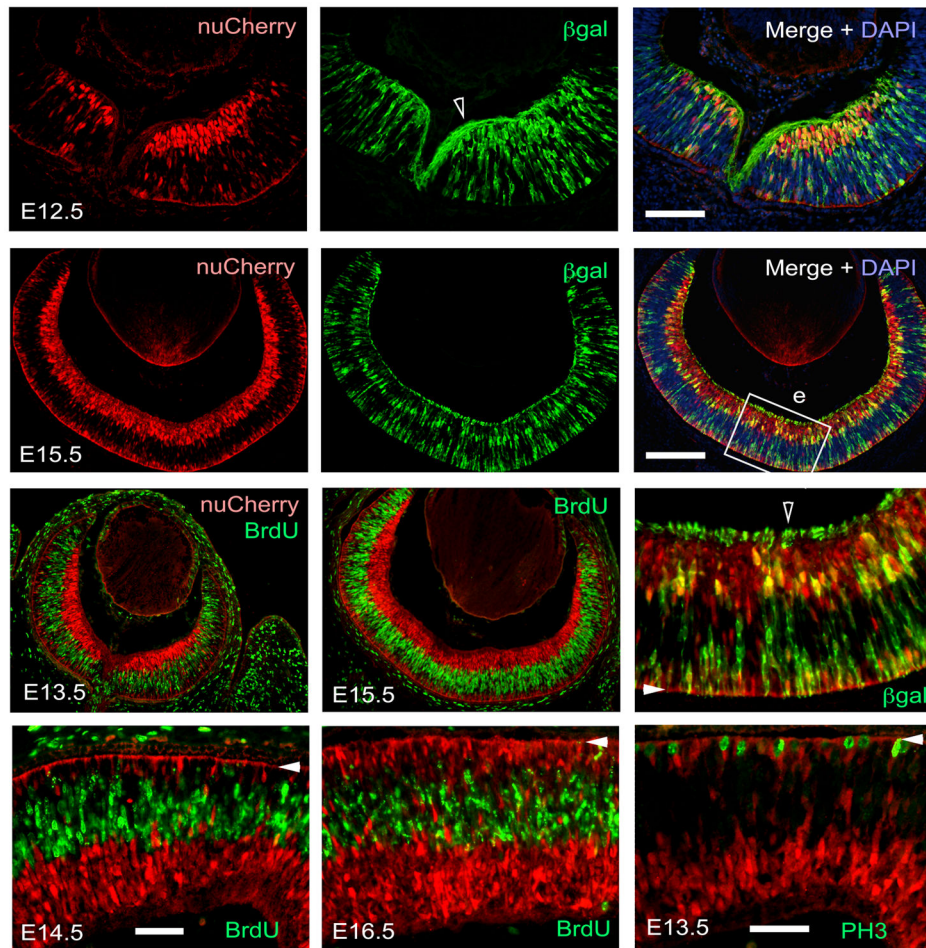
Figure 6.
Activity of the remote *ATOH7* retinal enhancer in 3034-BGnCherry mice. Double transgenic 3034-BGnCherry; *Math5-lacZ*/+ embryos were exposed to BrdU, harvested between E12 and E16, cryosectioned, and immunostained for nuCherry (red) and β-galactosidase, BrdU or phosphohistone H3 (green). **A,B,E.** The nuclear 3034- BGnCherry and cytoplasmic *Math5-lacZ* patterns are essentially overlapping, with >85% cell concordance (not shown). However, the subcellular localizations differ, with accumulation of βgal in RGC axons at the inner retinal surface and nascent optic nerve (open arrowheads). **C,D,F–H.** The 3034-BGnCherry transgene is expressed in post-mitotic retinal cells, with no overlap between nuCherry and the mitotic markers BrdU (S-phase) or PH3 (M-phase). Closed arrowheads mark the apical (sclerad) side in E–H. Scale bars: 40 μm in A; 20 μm in D; and 10 μm in E–H.
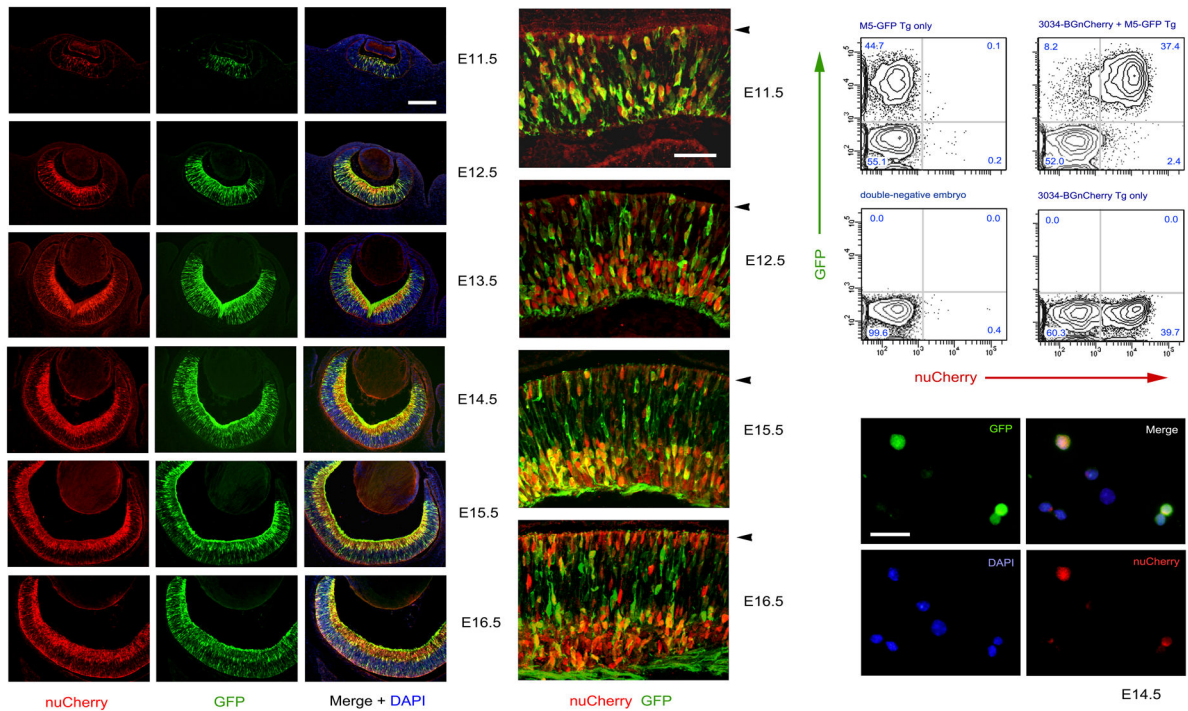
Figure 7.
Remote and primary *ATOH7* enhancers have similar activity in the developing mouse retina. Coexpression of nuCherry and GFP transgenes. **A–B.** Double transgenic 3034-BGnCherry; Math5-GFP embryos immunostained for both reporters. Low (**A**) and confocal high (**B**) magnification views of E11.5 to E16.5 retinal sections. The onset and expression patterns of the transgenes are essentially overlapping. **C.** Two-dimensional flow cytometric analysis of dissociated E14.5 retinal cells from 3034-BGnCherry × Math5-GFP littermate embryos carrying one, neither or both transgenes. The percentage of cells in each quadrant is indicated in the contour plots. The concordance between nuCherry and GFP fluorescence is high. Double-positive cells represent ~40% of the neural retina in 3034-BGnCherry; Math5-GFP embryos (upper right). **D.** Dissociated cells from an E14.5 double transgenic embryo immunostained for nuCherry and GFP. Arrowheads in B mark the apical side. Scale bars: 40 µm in A; 20 µm in B; and 10 µm in D.
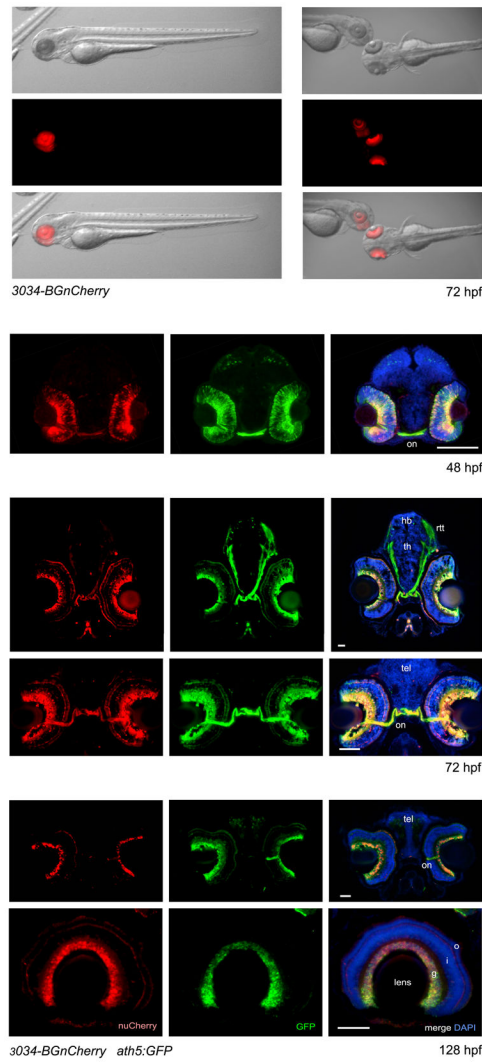
Figure 8.
The human remote *ATOH7* enhancer functions in developing zebrafish. **A,B.** Lateral and dorsal views of live embryos showing specific retinal expression of the *3034-BGnCherry* transgene in progenitor cells at 72 hpf development. **C–E.** Transverse sections of immunostained *3034-BGnCherry; ath5:GFP* embryos showing colocalized expression of nuCherry and GFP in the retina at 48, 72 and 128 hpf, with perdurance of reporter proteins in RGCs. The cytoplasmic GFP also labels RGC axons in the optic nerves, chiasm and tracts projecting to the thalamus and tectum. g, ganglion cell layer; hb, habenula; i, inner nuclear layer; o, outer nuclear layer; on, optic nerve; rtt, retinotectal tract; tel, telencephalon; th, thalamus; hpf, hours post fertilization. Scale bars, 50 μm.